**Kotelnikov A.R.[1], Suk N.I.[1], Kotelnikova Z.A.[1,2] Methods for evaluation of TP-parameters of processes in the Earth's crust (according to experimental studies).** UDC: 552.11, 550.4.02

[1]IEM RAS, Chernogolovka Moscow district, (kotelnik@iem.ac.ru); [2]IGPMG RAS, Moscow (kotelnik@igem.ru)

***Abstract.*** This paper provides a summary of methods for estimating the TP-parameters of natural processes based on experimental study of: (1) the interphase distribution of major, minor, rare elements and isotopes; (2) the distribution of elements between nonequivalent positions in the structure of minerals; (3) phase relationships in fluid inclusions in rock-forming minerals. The complex use of various methods makes it possible to estimate the TP-parameters of mineral genesis for almost all rocks of igneous and metamorphic genesis. The practical application of this approach for assessing the conditions of the genesis of various natural formations is shown.

*Keywords:TP-parameters, interphase distribution of elements, mineral genesis*

All thermometry methods are based on the concept of thermodynamic equilibrium. An analysis of mineral paragenesis from the point of view of the phase rule showed that the achievement of thermodynamic equilibrium in natural processes is quite common. In addition, studies of the interphase distribution of small elements and isotopes showed that they are also distributed according to the conditions of thermodynamic equilibrium. The study of the processes of crystallization of igneous rocks, mainly basalts of various genesis, showed that the distribution of elements in melt – mineral systems can also be described from the standpoint of equilibrium thermodynamics. Studies of phase equilibria in impact (ultrafast) processes show that the synthesized minerals are in a state of phase correspondence.

Thus, we can conclude that the phase correspondence method can be applied in various processes typical of petrogenesis in the lithosphere (magmatic, metamorphic, hydrothermal, etc.).

Consider the rates of chemical reactions, they are described by the following equations:

$V_r = dC_i/dt$; where $V_r$ – the rate of a chemical reaction, $C_i$ – the concentration of the i-th element, t – the time.

The reaction rate depends on the concentration of the reactants:

$V_r = k_0 * C_i^n * C_j^m$ ; where $C_{i,j}$ – component concentrations i,j; $k_0$ – reaction constant; n, m – reaction orders for the respective components.

For heterophase reactions, the reaction rate also depends linearly on the contact area of the two phases: $V_r \sim a*S$; where S – the contact area of two phases; a – coefficient depending on the nature of the substance.

The dependence of the reaction constant on temperature is determined by the following relationship: $k_0 * e^{-E/RT}$; where E is the activation energy of the reaction.

The general dependence of the reaction rate on temperature and concentration of reagents is:

$V_r = k_0 * \{e^{-E/RT}\} * C_i^n * C_j^m$.

On the whole, it can be concluded that the rates of distribution of elements between phases (minerals) depend on the concentration of components, temperature, and pressure.

It is clear that for the equilibria of the main rock-forming elements (Na, Mg, K, Ca, Mn, Fe), which form most of the minerals – solid solutions, the reaction rates of intermineral exchange equilibria are relatively high; while for impurity (Rb, Sr, Ba, Ni, Co, Cr, ... La ... Lu, Hf) elements and oxygen isotopes $^{17}O$, $^{18}O$, often used for thermometry, the reaction rates are low.

Therefore, when the PT-parameters of mineral genesis change (for example, due to a decrease in pressure during ascent and a decrease in temperature), reactions involving macro- and microelements will reflect this change in parameters in different ways.

(1) Reactions involving small elements (and isotopes) will capture the initial stages of the process (which are characterized by higher TP-parameters).

(2) Reactions involving the main elements will make it possible to track various stages of the process, which will be recorded in the zoning of minerals, the change in mineral generations, etc.

An analysis of the experimental data on cation exchange equilibria showed a significant dependence of the reaction rates on the coordination of the isomorphic ion. Table 1 shows semi-quantitative data on the rates of reactions of minerals. It follows from the data in Table 1 that the possibility of ion exchange is limited by the coordination number CN $\geq$ 8. Cation exchange through the recrystallization process is possible at CN=6. At CN=4 (tetrahedral position) the exchange is practically impossible, such systems can be studied only by the synthesis method.

Let us consider the methods used for the reconstruction of TPX-parameters of mineralogenesis:

- mineral thermobarometry based on the distribution of elements (isotopes) between

coexisting phases, as well as between non-equivalent positions of the structure of minerals (Table 2);

- study of fluid inclusions in minerals;
- study of the distribution of various (ore, petrogenic and volatile) components in mineral – fluid; melt – fluid; mineral – melt systems, etc.;
- experimental study of complex fluid-magmatic systems;
- a comprehensive study of characteristic natural objects.

Consider exchange equilibria of the form:

$3Mg_2Al_4Si_5O_{18} + 2Fe_3Al_2Si_3O_{12} = 2Mg_3Al_2Si_3O_{12} + 3Fe_2Al_4Si_5O_{18}$,

or:

$Crd^{Mg} + Alm = Prp + Crd^{Fe}$,

$NaAlSiO_4 + KAlSi_3O_8 = KAlSiO_4 + NaAlSi_3O_8$, or: Ne + San = Ks + Ab.

These equilibria have a large thermal effect and small volume effects, so they are used to determine the temperatures of mineral genesis. Exchange rates are quite high and these equilibria respond to temperature changes.

Fe-Mg-cordierite is usually stable in divariant association with *garnet, sillimanite, and quartz*:

$3(Mg,Fe)_2Al_4Si_5O_{18} = 2(Mg,Fe)_3Al_2Si_3O_{12} + 4Al_2SiO_5 + 5SiO_2$.

This reaction is accompanied by a very large volumetric effect and therefore underlies one of the most important geobarometers of metamorphic rocks.

**Table 1.** Rates of mineral cation exchange reactions depending on the structural position (coordination number) of an isomorphic cation**.**

| Mineral | Isomorphic cation | CN | Rate and type of cation exchange reactions |
|---|---|---|---|
| Zeolites | Na, Cs | 10 – 12 | High (ion exchange) |
| Feldspars | Na, K, Ca, Rb, Sr, Ba | 7 – 9 | Medium (ion exchange, recrystallization) |
| Garnets | Ca, Mg, Fe, Mn | 8 | Medium - ion exchange possible(?) |
| Garnets | $Fe^{3+}$, $Al^{3+}$, $Cr^{3+}$, $Ga^{3+}$ | 6 | Low (recrystallization) |
| Epidotes | $Fe^{3+}$, $Al^{3+}$ | 6 | Low (recrystallization) |
| Biotites | Mg, Fe | 6 | Low (recrystallization) |
| Cordieritis | Mg, Fe | 6 | Low (recrystallization) |
| Clinopyroxenes | Mg, Fe, Mn | 6 | Low (recrystallization) |
| Feldspars | Al, B, $Fe^{3+}$, Ga, Si, Ge | 4 | Very low (synthesis of solid solutions) |

**Table 2.** Various mineral thermometers and their applicability in assessing the parameters of mineral genesis

| Reaction type | Exchange rates | Stages of mineralogenesis processes (with a decrease in TP-parameters, fixed by this reaction) |
|---|---|---|
| Interphase distribution of small (impurity) elements | low | High temperature |
| Intracrystalline distribution of elements | medium | High and medium temperature |
| Interphase distribution of oxygen isotopes | medium | High and medium temperature |
| Cation exchange reactions of the main elements (Na, Mg, K, Ca, Mn, Fe) | high | Medium and low temperature |

Cordierite-garnet-quartz-sillimanite thermobarometer has a very simple analytical expression:

P (bar) = T (12.768 - 4.312ln$K_{Mg}$) - 2064, where $K_{Mg}$ – magnesium partition coefficient equal to $X_{Mg}^{Crd}/X_{Mg}^{Grt}$.

Distribution of small (impurity) elements. Mineral thermometer based on the incorporation of $SiO_2$ into the structure of nepheline in the presence of feldspar. This thermometer shows only the formation temperature of nepheline paragenesis in equilibrium with feldspar, since excess silica is in coordination 4 and is not capable of exchange.

T°C = 100*(qm-1.86+15.23*XKNe)/ /(1.26-1.72*XKNe) ±30°C; qm – mol.% of quartz in nepheline.

To estimate the TP-parameters of various objects (mainly metamorphic massifs, oceanic basalts, main intrusions), there are a number of software packages, such as TWQ, Petrolog, Komagmat, Putyrka's computational methods, etc.

It is rather difficult to estimate the parameters of the evolution of granite intrusions (so far, they work mainly on the basis of data from the study of melt inclusions), alkaline syenites (a relatively small number of mineral thermometers can be used there).

Fluid inclusions in minerals. The method of studying fluid inclusions in minerals makes it possible to determine the parameters of mineral genesis based on fluid samples directly captured during mineral formation. The method allows to estimate fluid density, its composition and, in correlation with the methods of mineral thermometry, to provide information on the actual conditions for the formation of minerals and their associations. Using the methods of studying fluid inclusions, we can determine: (1) the density of the mineral-forming fluid; (2) total fluid salinity (in NaCl, equiv); (3) fluid composition (semi-quantitatively). Together with the data of mineral thermometry, this makes it possible to determine the TP-trend of the evolution of the object studied.

Determination of fluid composition during metamorphism processes. The following methods are used: 1) calculations of mineral equilibria; 2) assessment of the bulk composition of the fluid during the chromatographic (mass-spectral) study of various groups of fluid inclusions. Metamorphic rocks often contain inclusions of carbonate-silicate rocks (Khanka massif, Aldan massif, etc.). Carbonate-silicate parageneses contain the following minerals: calcite ($CaCO_3$), quartz ($SiO_2$), wollastonite ($CaSiO_3$), grossular ($Ca_3Al_2Si_3O_{12}$), scapolite ($Ca_3Al_6Si_6O_{24}$*[$CaCO_3$]), plagioclase ($CaAl_2Si_2O_8$), alkaline feldspar ($KAlSi_3O_8$), epidote ($Ca_2Al_3Si_3O_{12}$[OH]). Based on the reactions between these minerals, it is possible to estimate the volatility of carbon dioxide and water.

1. $3CaAl_2Si_2O_8 + CaSiO_3 + CO_2 = Ca_3Al_6Si_6O_{24}$*[$CaCO_3$] + $SiO_2$ (estimation of $f_{CO2}$)
2. $CaSiO_3 + CO_2 = CaCO_3 + SiO_2$ (estimation of $f_{CO2}$)
3. $3CaAl_2Si_2O_8 + CaSiO_3 + H_2O = 2Ca_2Al_3Si_3O_{12}[OH] + SiO_2$ (estimation of $f_{H2O}$)
4. $3CaAl_2Si_2O_8 + CaCO_3 + H_2O = 2Ca_2Al_3Si_3O_{12}[OH] + CO_2$ (estimation of $f_{H2O}$/ $f_{CO2}$)

To calculate the composition of the fluid, the following assumptions are made:

- the fluid consists mainly of gases of the C-O-H system ($CO_2$, CO, $CH_4$, $H_2$, $H_2O$, $O_2$)
- fluid components behave as fully mobile;
- minerals are in equilibrium with the fluid phase;
- the properties of a complex fluid are described by a model of an ideal mixture of real gases.

The following reactions are used (silicate-carbonate parageneses):

$CaSiO_3 + CO_2 = CaCO_3 + SiO_2$ (estimation of carbon dioxide fugacity)

Considering the presence of carbon (graphite) – it is common in metamorphic rocks – gas equilibria can be calculated:

$CO_2 + C = 2CO$ (estimation of carbon dioxide fugacity)

$CO + ½\ O_2 = CO_2$ (estimation of oxygen potential).

Next, a system of 3 equations is solved:

$2H_2O + C = CH_4 + O_2$

$H_2 + ½O_2 = H_2O$

$X(CO_2)+X(CH_4)+X(H_2O)+X(CO)+X(H_2)=1$

This system is best solved by an iterative method using a computer. As a result of calculations, we obtain the mole fractions of gases in the fluid.

To calculate the composition of fluids, one can also use the parageneses of metapelitic (high-alumina) metamorphic rocks: garnet + biotite + feldspar + sillimanite + quartz + magnetite + graphite.

The following calculation is used:

1. $(Mg,Fe)_3Al_2Si_3O_{12}$(garnet) + $KAlSi_3O_8$ (feldspar) + $H_2O = K(Mg,Fe)_3AlSi_3O_{10}[OH]_2$ (biotite) + $Al_2SiO_5$(sillimanite) + $SiO_2$ (quartz) (estimation of $f_{H2O}$);
2. $Al_2SiO_5$(sillimanite) + $2SiO_2$ + $Fe_3O_4$(magnetite) = $Fe_3Al_2Si_3O_{12}$(garnet) + ½ ($O_2$) (estimation of $f_{O2}$);
3. $H_2O = H_2 + ½O_2$ (estimation of $f_{H2}$);
4. $2H_2 + C = CH_4$ (estimation of $f_{CH4}$);
5. solving a system of 2 equations (for known values $f_{H2O}$, $f_{O2}$, $f_{H2}$, $f_{CH4}$) :

$C + ½\ O_2 = CO$

$CO + ½\ O_2 = CO_2$ taking into account the balance equation $X(CO_2)+X(CH_4)+X(H_2O)+X(CO)+X(H_2)=1$ the composition of the gaseous components of the fluid can be obtained.

Conclusions

1. The rates of ion exchange reactions depend on the concentration of reagents, temperature and pressure. In addition, the dependence of the ion exchange rate on the coordination of an isomorphic atom was shown experimentally.
2. The intervals of application of various equilibria for mineral genesis temperature estimates are shown.
3. The method of studying fluid inclusions in minerals makes it possible to determine the parameters of mineral genesis based on fluid samples directly captured during mineral formation.
4. This method makes it possible to estimate the density of the fluid, its composition and, in correlation with the methods of mineral thermometry, provide information on the actual conditions for the formation of minerals and their associations.
5. The possibility of calculating the compositions of the mineral-forming fluid based on the mineral – fluid equilibria, in combination with the TP-measurement of mineral equilibria, is shown.

6. Complex approach to the assessment of TPX-parameters of mineralogenesis makes it possible to determine the physicochemical conditions for the formation of various endogenous rocks. Determining the TPX-parameters of petrogenesis is extremely important for assessing the boundary conditions for conducting experiments.

The work was supported by the program FMUF-*2022-0003*.

## Shornikov S.I.[1], Yakovlev O.I.[1], Minaev O.I.[2] Thermodynamic properties of the $Na_2O$–$Al_2O_3$ melts.

[1]V. I. Vernadsky Institute of Geochemistry & Analytical Chemistry RAS, Moscow (sergey.shornikov@gmail.com)
[2]Rambler Group, Moscow

**Abstract.** Within the framework of the developed semi-empirical model, the calculations were made of thermodynamic properties of the $Na_2O$–$Al_2O_3$ melts in the temperature region 1200–2500 K. The calculated values of the oxide activities and the mixing energies of melts are compared with available information.

*Keywords: thermodynamic properties of oxide melts, evaporation, the $Na_2O$–$Al_2O_3$ system.*

The study of the evaporation of the $Na_2O$–$Al_2O_3$ of melts is of interest for understanding the abnormally low volatility of sodium oxide in the processes of melt evaporative differentiation (Yakovlev et al., 1997). In this regard, the thermodynamic properties of refractory sodium aluminates ($NaAlO_2$, $Na_2Al_{12}O_{19}$ and $NaAl_{11}O_{17}$) and their melts at high temperatures (more than 1800 K) are of particular importance. In addition to the listed sodium aluminates, $Na_5AlO_4$, $Na_7Al_3O_8$, $Na_{17}Al_5O_{16}$ and $NaAl_5O_8$ are mentioned in the literature (Zintl, Morawietz, 1938; Thery, Briancon, 1962; Barker et al., 1981, 1984). The phase diagram of the $Na_2O$–$Al_2O_3$ system is presented in Fig. 1. It based on the results of reviews (Lambotte, Chartrand, 2013; Utlak, Besmann, 2019), although there are other versions of this diagram (Pratskova, Tyurin, 2013).

According to Galakhov (1985), the differences in the variants of phase diagram of the $Na_2O$–$Al_2O_3$ system are due to methodological errors arising due to the peculiarities of the physicochemical properties of sodium aluminates (in particular, the chemisorption nature of the absorption of external gases by sodium aluminates, which leads to the formation of impurity compounds). It is possible that these circumstances explain the discrepancies in the definitions of the melting temperature of sodium aluminate $NaAlO_2$: 1923±20 K (Matignon, 1923), 2123±30 K (Schairer, Bowen, 1956), 2140±6 K (Weber, Venero, 1970).

The available experimental physico-chemical information is limited to few and contradictory studies of phase diagram (Weber, Venero, 1970) and the thermodynamic properties of $NaAlO_2$, as well as some compositions of the $Na_2O$–$Al_2O_3$ system (mainly by the EMF method) in the temperature range not exceeding 1300 K. The data obtained are considered in detail in theoretical reviews (Eriksson et al., 1993; Witthohn et al., 1997; Besmann, Spear, 2002; Yazhenskikh et al., 2006; Lambotte, Chartrand, 2013; Utlak, Besmann, 2019). The evaporation of $NaAlO_2$ at 1280–1640 K was studied by the Knudsen effusion mass spectrometric method (Popkov, Semenov, 1971) and the temperature dependence of the $p_{Na}$ partial pressure over the compound was determined. Petric and Chatillon (2000) used the same method to determine the $Na_2O$ activities in the region of compositions close to corundum at 1573 K.

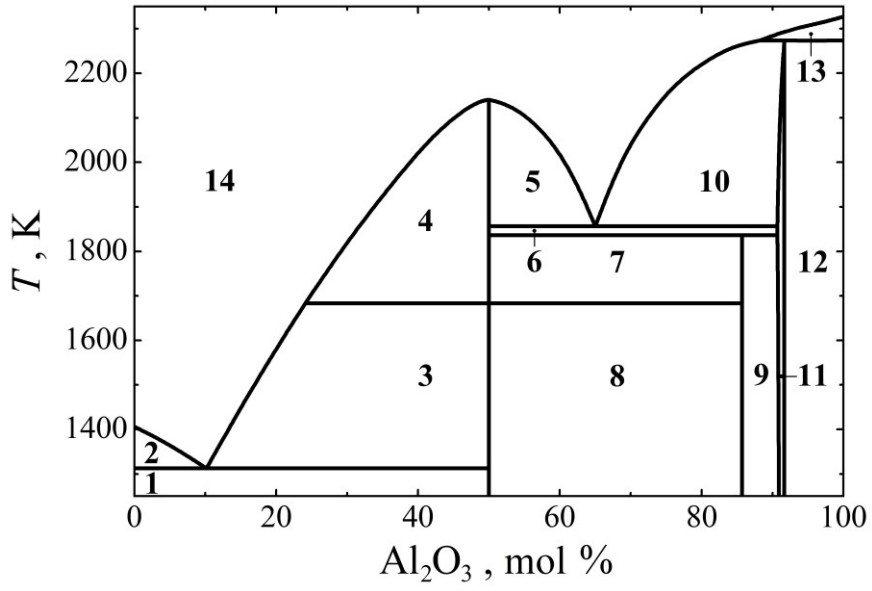


**Fig. 1.** The phase diagram of the $Na_2O$–$Al_2O_3$ system (Lambotte, Chartrand, 2013; Utlak, Besmann, 2019). List of symbols: 1 – α-$Na_2O$ + γ-$NaAlO_2$; 2 – α-$Na_2O$ + liquid; 3 – γ-$NaAlO_2$ + liquid; 4, 5 – δ-$NaAlO_2$ + liquid; 6 – δ-$NaAlO_2$ + β-$Na_2Al_{12}O_{19}$; 7 – δ-$NaAlO_2$ + β"-$Na_2Al_{12}O_{19}$; 8 – γ-$NaAlO_2$ + β"-$Na_2Al_{12}O_{19}$; 9 – β"-$Na_2Al_{12}O_{19}$ + $NaAl_{11}O_{17}$; 10 – β-$Na_2Al_{12}O_{19}$ + liquid; 11 – $NaAl_{11}O_{17}$; 12 – $NaAl_{11}O_{17}$ + $Al_2O_3$; 13 – $Al_2O_3$ + liquid; 14 – liquid

The results of calculations of oxide activity and mixing energy in the $Na_2O$–$Al_2O_3$ glasses at 1073 and 1473 K, performed by Besmann and Spear (2002) are shows in Fig. 2. They characterize the behavior of the mentioned sodium aluminates. The tendency to increase the mixing energy in the melts with increasing temperature corresponds to the accepted by Bale et al. (2016) of negative values of the enthalpies and entropies of the formation of $NaAlO_2$, $Na_2Al_{12}O_{19}$ and $NaAl_{11}O_{17}$ from oxides (Fig. 2b). However, the position of the minimum mixing energy does not correspond to the $NaAlO_2$ composition, as follows from the same data (Bale et al., 2016). Theoretical studies carried out by Eriksson et al. (1993), Yazhenskikh et al. (2006), Lambotte and Chartrand (2013) and Utlak and Besmann (2019) were devoted to the calculation of the phase diagram of the system and did not deal with the thermodynamic properties of sodium-aluminum melts.

The oxide activities and mixing energies in the $Na_2O$–$Al_2O_3$ melts at 1200–2500 K were calculated at the present study. The used semi-empirical model was described in detail earlier (Shornikov, 2019). The initial data for thermodynamic calculations were the accepted values (Bale et al., 2016) on the standard Gibbs energies of formation ($\Delta G°$) of simple oxides ($Na_2O$ and $Al_2O_3$) and sodium aluminates ($Na_5AlO_4$, $NaAlO_2$, $Na_2Al_{12}O_{19}$ and $NaAl_{11}O_{17}$) in the crystalline and liquid state, as well as information (Glushko et al., 1978–1982) on possible equilibria in the gas phase over the melt involving atomic and molecular forms (Na, $Na_2$, NaO, $Na_2O$, $Na_2O_2$, Al, AlO, $Al_2O$, $AlO_2$, $Al_2O_2$, $Al_2O_3$, O, $O_2$, $O_3$ and $O_4$). The $\Delta G°$ values of condensed phases and vapor species of the gas phase over the melt were used to find equilibrium conditions at a given melt composition and temperature.

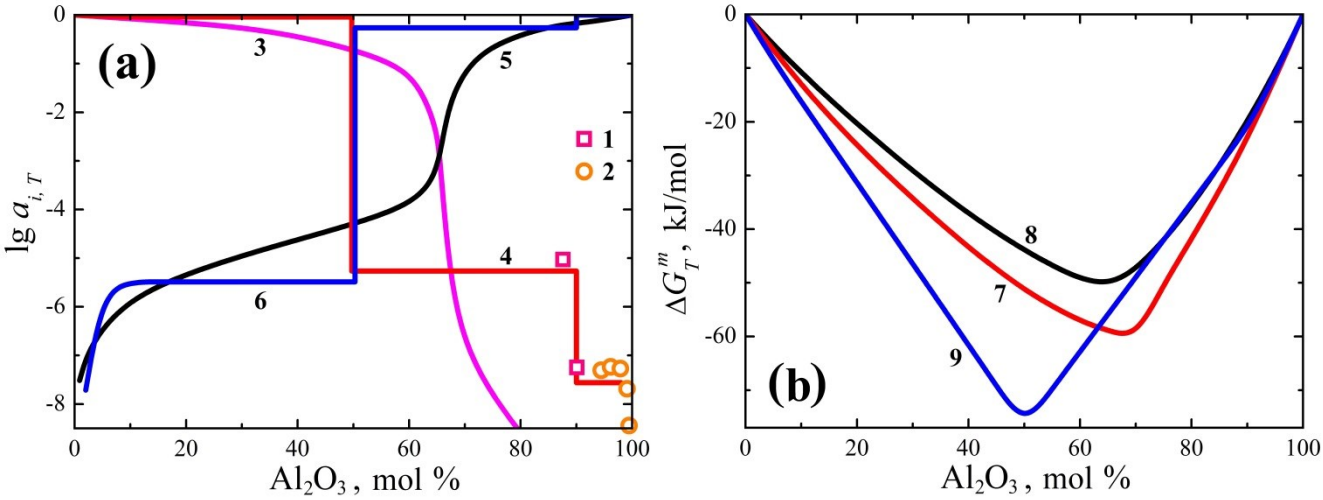


**Fig. 2.** The $Na_2O$ (1–4) and $Al_2O_3$ (5, 6) activities (a) and the mixing energy (7–9) (b) in the $Na_2O$–$Al_2O_3$ melts at 1073 (3, 5, 7), 1450 (1, 4, 6, 9), 1473 (8) and 1573 (2) K, determined experimentally: 1 (Witthohn et al., 1997) and 2 (Petric, Chatillon, 2000), as well as calculated: 3, 5, 7, 8 (Besmann, Spear, 2002) and at the present study (4, 6, 9).

As follows from Fig. 2, the results of calculations of the oxide activities in the $Na_2O$–$Al_2O_3$ system at 1450 K performed at the present study correspond to those accepted by Witthohn et al. (1997) on the basis of experimental data (Elrefaie, Smeltzer, 1981, 1984; Rog, Kozlowska-Rog, 1982; Rog et al.., 1983; Kale, Jacob, 1989; Jacob et al., 1991; Kale, 1992). They were obtained by the EMF method for compositions close to $Na_2Al_{12}O_{19}$ and $NaAl_{11}O_{17}$. The calculation results do not contradict the data obtained by Petric and Chatillon (2000). Typical changes in the concentration dependences of $Na_2O$ and $Al_2O_3$ activities in melts at 1450 K indicate the position of the liquid corresponding to the phase diagram (Fig. 1). The mixing energy minimum value is in the region of compositions close to the $NaAlO_2$ compound and is equal to –77 kJ/mol. The $Na_2O$ and $Al_2O_3$ activity values in the $Na_2O$–$Al_2O_3$ melts increase at 2300 K (Fig. 3a) at corresponding increase in the minimum mixing energy in the melt to –60 kJ/mol (Fig. 3b).

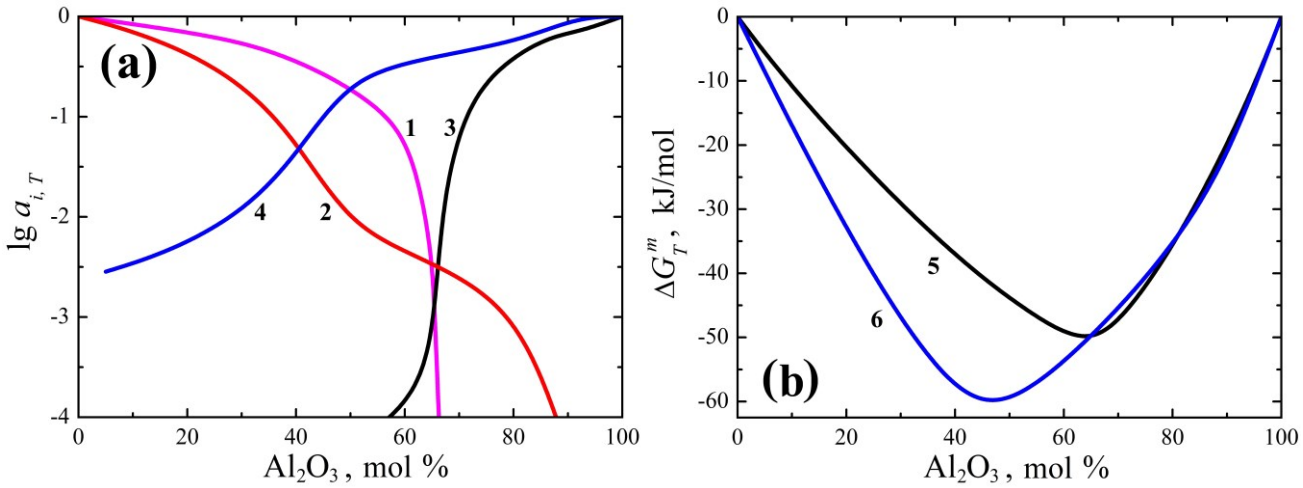


**Fig. 3.** The $Na_2O$ (1, 2) and $Al_2O_3$ (3, 4) activities (a) and the mixing energy (5, 6) (b) in the $Na_2O$–$Al_2O_3$ melts at 1073 (1, 3), 1473 (5) and 2300 (2, 4, 6) K calculated by: 1, 3, 5 (Besmann, Spear, 2002) and at the present study (2, 4, 6).

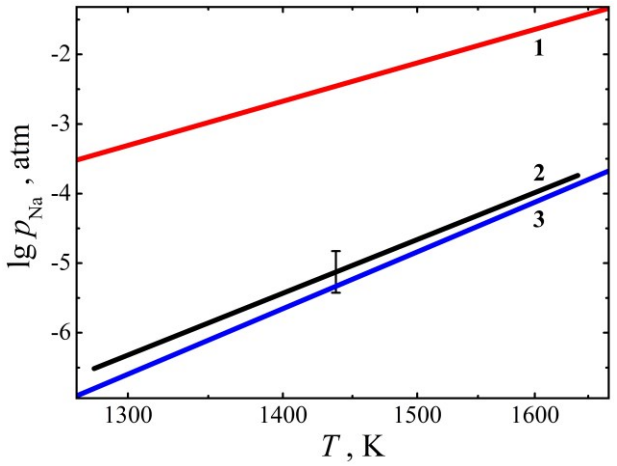


**Fig. 4.** The temperature dependences of the $p_{Na}$ partial pressure over $Na_2O$ (1) and $NaAlO_2$ (2, 3) are determined by: 1 – according to thermochemical data (Glushko et al., 1978–1982); 2 – the Knudsen effusion mass spectrometric method (Popkov, Semenov, 1971) and 3 – calculated at the present study.

The calculated atomic sodium partial pressures over the $NaAlO_2$ sodium aluminate, as follows from Fig. 4, correspond satisfactorily to the experimental data obtained by the Knudsen effusion mass spectrometric method (Popkov, Semenov, 1971). Comparison of the $p_{Na}$ partial pressures over sodium oxide with those over the $NaAlO_2$ sodium aluminate (Fig. 4) shows its excess by $10^3$ times, which probably causes the low volatility of sodium oxide in the processes of the melt evaporative differentiation.

### References


Bale C. W., Belisle E., Chartrand P., Degterov S. A., Eriksson G., Gheribi A. E., Hack K., Jung I.-H., Kang Y.-B., Melancon J., Pelton A. D., Petersen S., Robelin C., Sangster J., Spencer P., VanEnde M.-A. (2016) FactSage thermochemical software and databases – recent developments 2010–2016. *CALPHAD*, vol. 54, no. 1, pp. 35–53.

Barker M. G., Gadd P. G., Begley M. J. (1981) Preparation and crystal structures of the first alkali-rich sodium aluminates $Na_7Al_3O_8$ and $Na_5AlO_4$. *J. Chem. Soc., Chem. Comm.*, vol. 8, pp. 379–381.

Barker M. G., Gadd P. G., Begley M. J. (1984) Identification and characterisation of three novel compounds in the sodium – aluminium – oxygen system. *J. Chem. Soc. Dalton Trans.*, vol. 6, pp. 1139–1146.

Besmann T. M., Spear K. E. (2002) Thermochemical modeling of oxide glasses. *J. Amer. Ceram. Soc.*, vol. 85, no. 12, pp. 2887–2894.

Elrefaie F. A., Smeltzer W. W. (1981) The stability of β-$Al_2O_3$ ($Na_2O \cdot 11Al_2O_3$) in oxygen atmospheres. *J. Electrochem. Soc.*, vol. 128, no. 7, pp. 1443–1447.

Elrefaie F. A., Smeltzer W. W. (1984) Thermodynamic properties of the ionic conducting phases of Na–Al–O system between 800 and 1200 K. *Solid State Ionics*, vol. 12, pp. 517–524.

Eriksson G., Wu P., Pelton A. D. (1993) Critical evaluation and optimization of the thermodynamic properties and phase diagrams of the MgO–$Al_2O_3$, MnO–$Al_2O_3$, FeO–$Al_2O_3$, $Na_2O$–$Al_2O_3$ and $K_2O$–$Al_2O_3$ systems. *CALPHAD*, vol. 17, no. 2, pp.189–205.

Galakhov F. Y. (1985) Phase diagrams of refractory oxide systems. The binary systems. Leningrad: Nauka, vol. 5, pt. 1, 284 pp. [in Russian].

Glushko V. P., Gurvich L. V., Bergman G. A., Veitz I. V., Medvedev V. A., Khachkuruzov G. A., Yungman V. S. (1978–1982) Thermodynamic properties of individual substances. Moscow: Nauka, vol. 1–4 [in Russian].

Jacob K. T., Swaminathan K., Sreedharan O. M. (1991) Potentiometric determination of activities in the two-phase fields of the system $Na_2O$–(α)$Al_2O_3$. *Electrochim. Acta*, vol. 36, no. 5–6, pp. 791–798.

Kale G. M. (1992) $Na_2O$–$Al_2O_3$ system: activity of $Na_2O$ in (α+β)- and (β+β")-alumina. *Met. Trans. B*, vol. 23, no. 6, pp. 833–839.
Kale G. M., Jacob K. T. (1989) Thermodynamic stability of K β-alumina. *Met. Trans. B*, vol. 20, no. 5, pp. 687–691.
Lambotte G., Chartrand P. (2013) Thermodynamic modeling of the ($Al_2O_3$ + $Na_2O$), ($Al_2O_3$ + $Na_2O$ + $SiO_2$), and ($Al_2O_3$ + $Na_2O$ + $AlF_3$ + NaF) systems. *J. Chem. Thermodyn*., vol. 57, pp. 306–334.
Matignon C. (1923) Action des temperatures elevees sur quelques substances refractaires. *C. R. Acad. Sci. Paris*, vol. 177, no. 24, pp. 1290–1293.
Petric A., Chatillon C. (2000) Dilute activity coefficients and solubility in binary oxides by mass spectrometry: the $Na_2O$–$Al_2O_3$ and MgO–$Al_2O_3$ systems. *High Temperature Materials Chemistry*, vol. 2, pp. 415–418.
Popkov O. S., Semenov G. A (1971) Mass spectrometric study of evaporation of lithium and sodium aluminates. *Russ. J. Phys. Chem*., vol. 45, no. 2, pp. 476–477.
Pratskova S. E., Tyurin A. G. (2013) Phase equilibria involving oxide-fluoride melts of sodium and aluminium. *Butlerov Comm*., vol. 36, no. 12, pp. 163–167.
Rog G., Kozlowska-Rog A. (1982) Thermodynamic properties of sodium polyaluminates. *Solid State Ionics*, vol. 7, no. 4, pp. 291–294.
Rog, G., Kozinski S., Kozlowska-Rog A. (1983) The application of NASICON ($Na_3Zr_2Si_2PO_{12}$) to the thermodynamic study of beta-alumina. *Electrochim. Acta*, vol. 28, no. 1, pp. 43–45.
Schairer J. F., Bowen N. L. (1956) The system $Na_2O$–$Al_2O_3$–$SiO_2$. *Amer. J. Sci*., vol. 254, no. 3, pp. 129–195.
Shornikov S. I. (2019) Thermodynamic modelling of evaporation processes of lunar and meteoritic substance. *Geochem. Int*., vol. 57, no. 8, pp. 865–872.
Thery J., Briancon D. (1962) Sur les proprietes d'un nouvel aluminate de sodium $NaAl_5O_8$. *C. R. Acad. Sci. Paris*, vol. 254, no. 15, pp. 2782–2784.
Utlak S. A., Besmann T. M. (2018) Thermodynamic assessment of the pseudoternary $Na_2O$–$Al_2O_3$–$SiO_2$ system. *J. Amer. Ceram. Soc*., vol. 101, no. 2, pp. 928–948.
Weber N., Venero A. F. (1970) Revision of the phase diagram $NaAlO_2$–$Al_2O_3$. *Amer. Ceram. Soc. Bull*., vol. 49, no. 4, pp. 491–492.
Witthohn A., Oeltjen L., Hilpert K. (1997) Massenspektrometrische untersuchungeb und thermochemische modellrechnungen zur freisetzung und einbindung von alkalien bei der kohleunwandlung. *Ber. Forschung*. Julich, Institute fur Werkstoffe der Energietechnik, Jul-3366, 60 pp.
Yakovlev O. I., Dikov Y. P., Gerasimov M. V., Wlotzka F. (1997) Peculiarities of aluminum volatilization from silicate melts. *Geochem. Int*., vol. 35, no. 12, pp. 1046–1059.
Yazhenskikh E., Hack K., Muller M. (2006) Critical thermodynamic evaluation of oxide systems relevant to fuel ashes and slags. Part 2: alkali oxide – alumina systems. *CALPHAD*, vol. 30, no. 4, pp. 397–404.
Zintl E., Morawietz W. (1938) Orthosalze von sauerstoffsauren. *Z. anorg. allg. Chem*., vol. 236, no. 1–4, pp. 372–410.

## Shornikov S.I.[1], Slobodov A.A.[2] Thermodynamic properties of the $K_2O$ – $Al_2O_3$ melts.

[1] V. I. Vernadsky Institute of Geochemistry & Analytical Chemistry RAS, Moscow, (sergey.shornikov@gmail.com)
[2] Saint Petersburg State Institute of Technology, St. Petersburg

**Abstract.** Within the framework of the developed semi-empirical model, the calculations were made of thermodynamic properties of the $K_2O$–$Al_2O_3$ melts in the temperature region 1200–2500 K. It is shown that at 2300 K, the mixing energies of potassium–aluminum melts are minimal in a number of other aluminate melts ($Na_2O$–$Al_2O_3$, CaO–$Al_2O_3$, MgO–$Al_2O_3$, $SiO_2$–$Al_2O_3$, $TiO_2$–$Al_2O_3$ and FeO–$Al_2O_3$).

*Keywords: thermodynamic properties of oxide melts, evaporation, the $Na_2O$–$Al_2O_3$ system.*

The relative volatility of alkaline oxides ($Na_2O$ and $K_2O$) during the melt evaporation is the subject of numerous geochemical and cosmochemical studies. The results of studies of evaporative differentiation of melts under the action of high-speed impact (Yakovlev et al., 1988) are shows the relative content of alkalis in the melt can both increase and decrease depending on the initial content of silicate and aluminate parts in the melt (Fig. 1).

The study of the thermodynamic properties of the $K_2O$–$Al_2O_3$ system is of particular interest both for understanding the abnormally low volatility of potassium oxide in the processes of melt evaporation, and for solving technical problems of high-temperature corrosion in the MHD generator operations. The existence of refractory potassium aluminates – $KAlO_2$, $K_2Al_{12}O_{19}$ and $KAl_9O_{14}$ has been established in the $K_2O$–$Al_2O_3$ system, but information is quite contradictory. Thus, according to the data obtained by Roth (1980) and Moya et al. (1982), the $KAlO_2$ melting point is above 2500 K. It seems to be an overestimated value compared to the one accepted by Glushko et al. (1982), equal to 1986±10 K. Variants of the $K_2O$–$Al_2O_3$ phase diagram are presented in Fig. 2 based on the reviews (Kim et al., 2018; Nekhoroshev, 2019; Utlak, 2019) and (Eliezer, Howald, 1978; Schamm et al., 1990). In addition to the listed potassium aluminates, $K_5AlO_4$ and $K_3AlO_3$ are mentioned in (Bon et al., 1974). They dissociate at low temperatures.

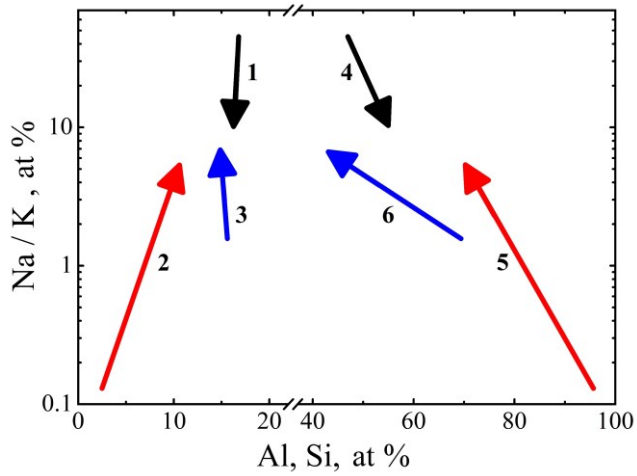


**Fig. 1.** The change in the Na / K atomic ratio *vs*. the Al (1–3) and Si (4–6) atomic content in the composition of the target and the condensate of basalt (1, 4), quartzite (2, 5) and obsidian (3, 6) formed during evaporation under the action of a high-speed impact (Yakovlev et al., 1988). The arrow indicates the change in the initial composition of the target to the composition of the formed condensate.

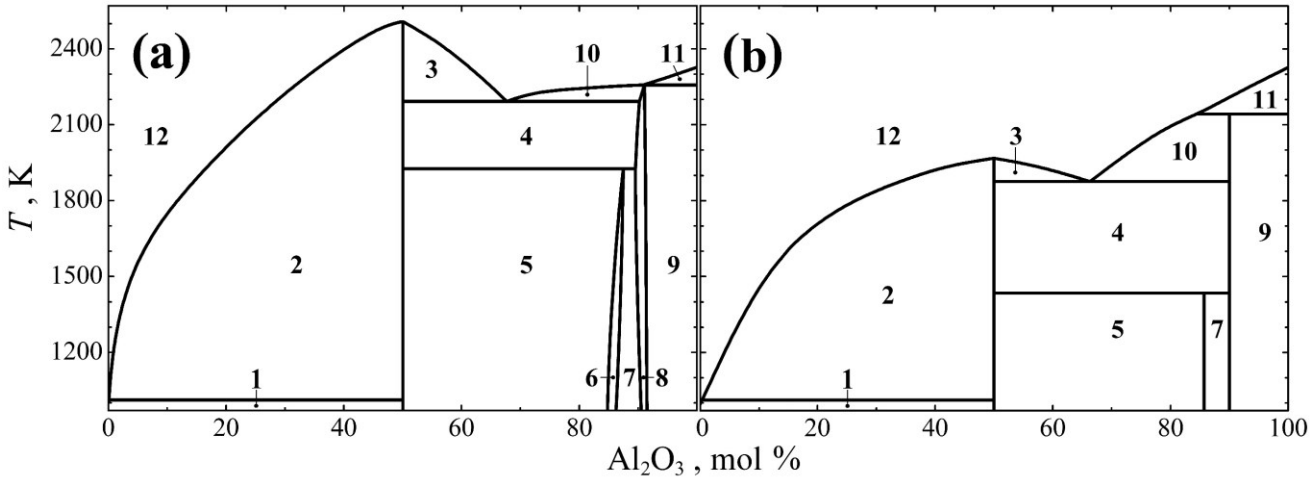


**Fig. 2.** The phase diagram of the $K_2O$–$Al_2O_3$ system: (a) – according to Kim et al. (2018), Nekhoroshev (2019) and Utlak (2019), and (b) – according to Eliezer and Howald (1978) and Schamm et al. (1990). List of symbols: 1 – $K_2O$ + $KAlO_2$; 2, 3 – $KAlO_2$ + liquid; 4 – $KAlO_2$ + $KAl_9O_{14}$; 5 – $KAlO_2$ + $K_2Al_{12}O_{19}$; 6 – $K_2Al_{12}O_{19}$ (solid solution); 7 – $K_2Al_{12}O_{19}$ + $KAl_9O_{14}$; 8 – $KAl_9O_{14}$ (solid solution); 9 – $KAl_9O_{14}$ + $Al_2O_3$; 10 – $KAlO_2$ + $KAl_9O_{14}$ + liquid; 11 – $Al_2O_3$ + liquid; 12 – liquid.

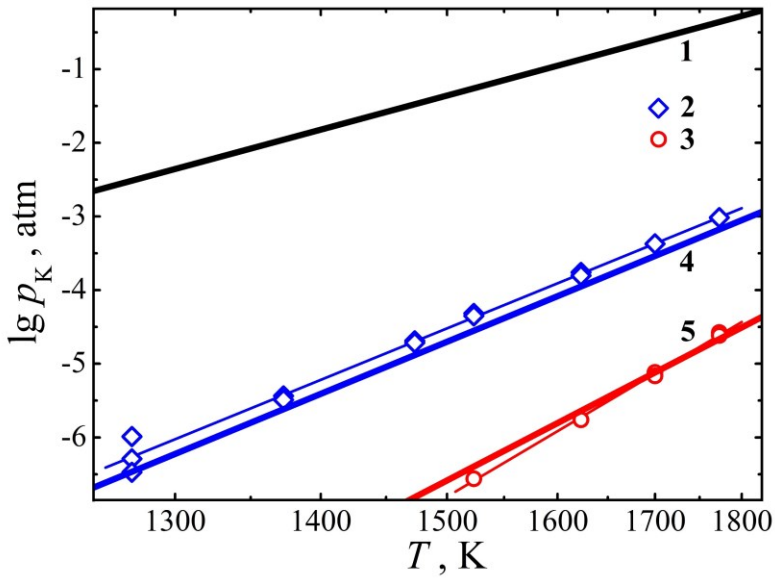


**Fig. 3.** The temperature dependences of the $p_K$ partial pressure over $K_2O$ (1), $K_2Al_{12}O_{19}$ (2, 4) and $KAl_9O_{14}$ (3, 5) are determined by: 2 and 3 – the Knudsen effusion mass spectrometric method (Plante et al., 1975) and 1, 4, 5 – calculated at the present study.

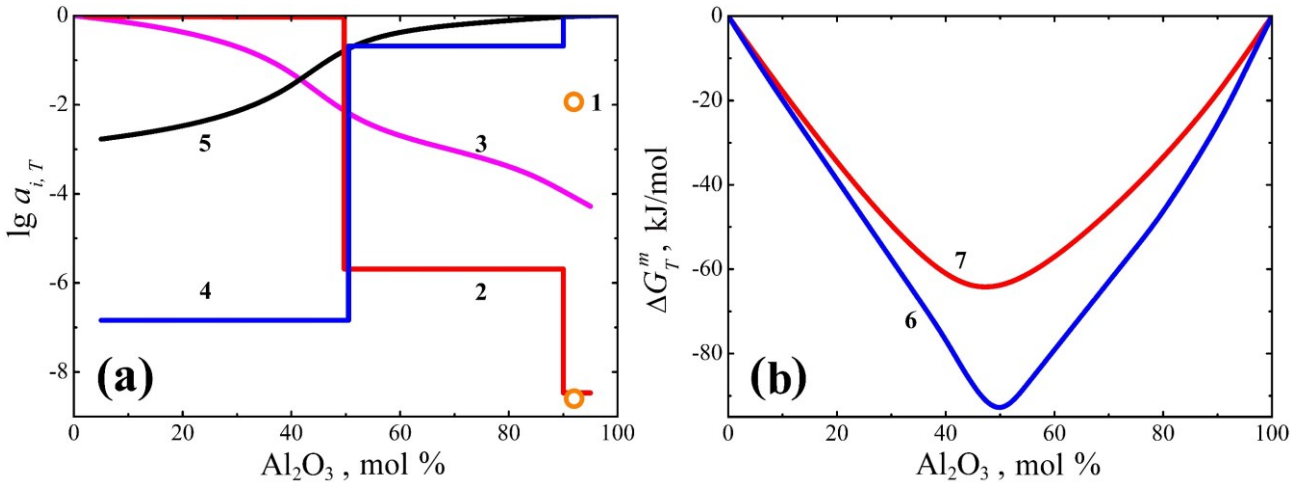


**Fig. 4.** The $K_2O$ (1–3) and $Al_2O_3$ (4, 5) activities (a) and the mixing energy (6, 7) (b) in the $K_2O$–$Al_2O_3$ melts at 1450 (1, 2, 4, 6) and 2300 (3, 5, 7) K, determined experimentally: 1 (Witthohn et al., 1997), as well as calculated at the present study (2–7).

The available physicochemical data on the compounds and the $K_2O$–$Al_2O_3$ melts are reviewed in (Glushko et al., 1982; Berezhnoy, 1988; Eriksson et al., 1993; Witthohn et al., 1997; Yazhenskikh et al., 2006; Bale et al., 2016). The evaporation of compositions close to $K_2Al_{12}O_{19}$ and $KAl_9O_{14}$ was studied by the Knudsen effusion mass spectrometric method at 1273–1773 K and the temperature dependences of the $p_K$ partial pressures (Fig. 3) were determined (Plante et al., 1975).

The oxide activities and mixing energies in the $K_2O$–$Al_2O_3$ melts at 1200–2500 K were calculated at the present study. The used semi-empirical model was described in detail earlier (Shornikov, 2019) The initial data for thermodynamic calculations were the standard Gibbs energies of formation ($\Delta G°$) of simple oxides ($K_2O$ and $Al_2O_3$) and potassium aluminates ($K_5AlO_4$, $KAlO_2$, $K_2Al_{12}O_{19}$ and $KAl_9O_{14}$) in the crystalline and liquid state (Beyer et al., 1980; Glushko et al., 1982; Bennington, Daut, 1988; Bale et al., 2016), as well as information on possible equilibria in the gas phase over the melt involving the vapor species (K, $K_2$, KO, $K_2O$, $K_2O_2$, Al, AlO, $Al_2O$, $AlO_2$, $Al_2O_2$, $Al_2O_3$, O, $O_2$, $O_3$, $O_4$ and KAlO). Thermodynamic data characterizing the KAlO vapor specie were taken from (Farber et al., 1986). The $\Delta G°$ values of condensed phases and the vapor species of the gas phase over the melt were used to find equilibrium conditions for a given melt composition and temperature.

The results of calculations of the oxide activities in the $K_2O$–$Al_2O_3$ system at 1450 K correspond to those accepted by Witthohn et al. (1997) on the basis of experimental data (Itoh, Kozuka, 1988; Kale, Jacob, 1989) obtained by the EMF method for the $KAl_9O_{14}$ compound (Fig. 4a). The minimum value of the mixing energy in the $K_2O$–$Al_2O_3$ system is close to the $KAlO_2$ composition and is equal to –95 kJ/mol (Fig. 4b). The $K_2O$ and $Al_2O_3$ activities in the $K_2O$–$Al_2O_3$ melts at 2300 K are increase (Fig. 4a) and we can see a corresponding increase in the mixing energy minimum in the $KAlO_2$ melt to –65 kJ/mol (Fig. 4b).

The calculated atomic potassium partial pressures over the $K_2Al_{12}O_{19}$ and $KAl_9O_{14}$ potassium aluminates (Fig. 3) correspond satisfactorily to the experimental data obtained by the Knudsen effusion mass spectrometric method (Plante et al., 1975). The partial pressures of the KAlO vapor specie over the $K_2O$–$Al_2O_3$ melts are increase significantly with temperature increasing, however do not exceed $3.5\times10^{-9}$ atm at 2300 K.

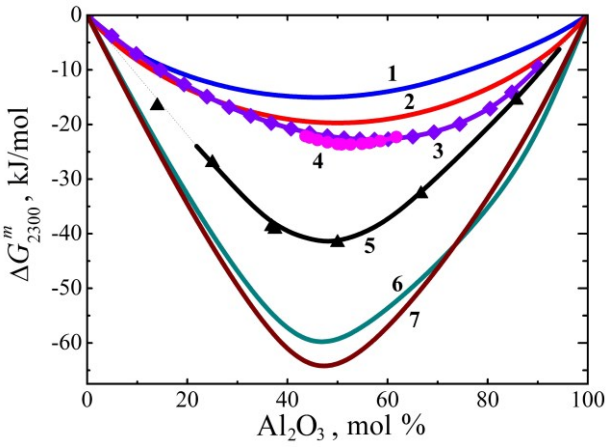


**Fig. 5.** The mixing energy in the aluminate melts at 2300 K: $FeO$–$Al_2O_3$ (1), $TiO_2$–$Al_2O_3$ (2), $SiO_2$–$Al_2O_3$ (3), $MgO$–$Al_2O_3$ (4), $CaO$–$Al_2O_3$ (5), $Na_2O$–$Al_2O_3$ (6) and $K_2O$–$Al_2O_3$ (7).

Comparison of mixing energies in the binary aluminate melts at 2300 K shows the minimum values for alkaline systems in the following series: $FeO$–$Al_2O_3$ (Shornikov, 1997), $TiO_2$–$Al_2O_3$ (Shornikov, Shornikova, 2018), $SiO_2$–$Al_2O_3$

(Shornikov, Archakov, 2000), $MgO–Al_2O_3$ (Shornikov, 2018), $CaO–Al_2O_3$ (Shornikov et al., 1997), $Na_2O–Al_2O_3$ and $K_2O–Al_2O_3$ (Fig. 5).

**References**


Bale C. W., Belisle E., Chartrand P., Degterov S. A., Eriksson G., Gheribi A. E., Hack K., Jung I.-H., Kang Y.-B., Melancon J., Pelton A. D., Petersen S., Robelin C., Sangster J., Spencer P., VanEnde M.-A. (2016) FactSage thermochemical software and databases – recent developments 2010–2016. *CALPHAD*, vol. 54, no. 1, pp. 35–53.

Bennington K. O., Daut G. E. (1988) The standard formation data for $KAlO_2$. *Thermochim. Acta*, vol. 124, pp. 241–245.

Berezhnoi A. S. (1988) Multicomponent alkaline oxide systems. Kiev: Naukova dumka, 200 p.

Beyer R. P., Ferrante M. J., Brown R. R. (1980) Thermodynamic properties of $KAlO_2$. *J. Chem. Thermodyn*., vol. 12, no. 10, pp. 985–991.

Bon A., Gleitzer C., Courtois A., Protas J. (1974) Synthese et structure cristalline d'un nouvel aluminate de potassium. *C. R. Acad. Sci. Paris*, vol. 278, no. 11, pp. 785–788.

Eliezer I., Howald R. A. (1978) High-temperature thermodynamics and phase equilibria in the potassium oxide – aluminum oxide system. *High Temp. Sci*., vol. 10, pp. 1–16.

Eriksson G., Wu P., Pelton A. D. (1993) Critical evaluation and optimization of the thermodynamic properties and phase diagrams of the $MgO–Al_2O_3$, $MnO–Al_2O_3$, $FeO–Al_2O_3$, $Na_2O–Al_2O_3$ and $K_2O–Al_2O_3$ systems. *CALPHAD*, vol. 17, no. 2, pp.189–205.

Farber M., Srivastava R., Moyer J., Leeper J. (1986) Effusion-mass spectrometric determination of the thermodynamic properties of KAlO (g) and KSiO (g). *High Temp. Sci*., vol. 21, no. 1, pp. 17–26.

Glushko V. P., Gurvich L. V., Bergman G. A., Veitz I. V., Medvedev V. A., Khachkuruzov G. A., Yungman V. S. (1982) Thermodynamic properties of individual substances. Moscow: Nauka, vol. 4, pt. 1 and 2 [in Russian].

Itoh M., Kozuka Z. (1988) Thermodynamic stability of potassium $K^+$-β-alumina. *J. Amer. Ceram. Soc*., vol. 71, no. 1, pp. C36–C39.

Kale G. M., Jacob K. T. (1989) Thermodynamic stability of potassium β-alumina. *Met. Trans. B*, vol. 20, no. 5, pp. 687–691.

Kim D.-G., Moosavi-Khoonsari E., Jung I.-H. (2018) Thermodynamic modeling of the $K_2O–Al_2O_3$ and $K_2O–MgO–Al_2O_3$ systems with emphasis on β- and β″-aluminas. *J. Eur. Ceram. Soc*., vol. 38, pp. 3188–3200.

Moya J. S., Criado E., De Aza S. (1982) The $K_2O \cdot Al_2O_3–Al_2O_3$ system. *J. Mater. Sci*., vol. 17, no. 8, pp. 2213–2217.

Nekhoroshev E. (2019) Thermodynamic optimization of the $Na_2O–K_2O–Al_2O_3–CaO–MgO–B_2O_3–SiO_2$ system. *Thesis*, Universite de Montreal, 529 p.

Plante E. R., Olson C. D., Negas T. (1975) Interaction of $K_2O$ with slag in open cycle, coal fired MHD. VI Intern. conf. *Magnetohydrodynamic electrical power generation II*. Washington, pp. 211–218.

Roth R. S. (1980) Phase equilibria research in portions of the system $K_2O–MgO–Fe_2O_3–Al_2O_3–SiO_2$. *Solid state chemistry: a contemporary overview*, vol. 186, pp. 391–408.

Schamm S., Rabardel L., Grannec J., Naslain R. (1990) Partial phase diagram of the ternary reciprocal system $KF–AlF_3–Al_2O_3–K_2O$. *CALPHAD*, vol. 14, no. 4, pp. 385–402.

Shornikov S. I., Stolyarova V. L., Shultz M. M. (1997) A mass–spectrometric study of vapor composition and thermodynamic properties of $CaO–Al_2O_3$ melts. *Russ. J. Phys. Chem*., vol. 71, no. 1, pp. 19–22.

Shornikov S. I., Archakov I. Yu. (2000) A mass spectrometric study of the thermodynamic properties of $Al_2O_3–SiO_2$ melts. *Russ. J. Phys. Chem*., vol. 74, no. 5, pp. 684–688.

Shornikov S. I. (2017) Thermodynamic properties of the $FeO–Al_2O_3$ melts. XVIII Intern. conf. *Physico-chemical and petrophysical research in Earth sciences*, Moscow: IGEM, pp. 326–329 [in Russian].

Shornikov S. I., Shornikova M. S. (2018) Thermodynamic properties of the $Al_2O_3–TiO_2$ melts. XIX Intern. conf. *Physico-chemical and petrophysical research in Earth sciences*, Moscow: IGEM, pp. 349–352 [in Russian].

Shornikov S. I. (2018) Mass spectrometric study of the thermodynamic properties of spinel solid solutions. *Russ. J. Phys. Chem. A*, vol. 92, no. 8, pp. 1447–1456.

Shornikov S. I. (2019) Thermodynamic modelling of evaporation processes of lunar and meteoritic substance. *Geochem. Int*., vol. 57, no. 8, pp. 865–872.

Utlak S. A. (2019) Modeling complex oxides: thermochemical behavior of nepheline-forming Na–Al–Si–B–K–Li–Ca–Mg–Fe–O and hollandite-forming Ba–Cs–Ti–Cr–Al–Fe–Ga–O systems. *Thesis*, University of South Carolina, 260 p.

Witthohn A., Oeltjen L., Hilpert K. (1997) Massenspektrometrische untersuchungeb und thermochemische modellrechnungen zur freisetzung und einbindung von alkalien bei der kohleunwandlung. *Ber. Forschung*. Julich, Institute fur Werkstoffe der Energietechnik, Jul-3366, 60 pp.

Yakovlev O. I., Fainberg V. S., Kaznacheev E. A., Pilugin N. N., Baulin N. N., Tikhomirov S. G. (1988) Experimental study of evaporation at high-speed impact. *Geochem. Int*., vol. 25, no. 12, pp. 1698–1707.

Yazhenskikh E., Hack K., Muller M. (2006) Critical thermodynamic evaluation of oxide systems relevant to fuel ashes and slags. Part 2: alkali oxide – alumina systems. *CALPHAD*, vol. 30, no. 4, pp. 397–404.


## Voronin M.V., Osadchii E.G., Brichkina E.A., Osadchii V.O. The thermodynamic properties of krennerite ($AgAu_4Te_{10}$ or $AgAu_3Te_8$): EMF method with solid electrolyte $Ag_4RbI_5$.

D.S. Korzhinskii Institute of Experimental Mineralogy of Russian Academy of Sciences: brichkina@iem.ac.ru

**Abstract.** For the first time, the thermodynamic properties of krennerite ($AgAu_4Te_{10}$ and $AgAu_3Te_8$) were determined. The calculations of the thermodynamic functions were made from the temperature dependence of the electromotive force (EMF). The measurements were carried out in the field of Ag-Au-Te system by the method of EMF in a completely solid-state electrochemical cell with a common gas space:

(–) Pt| $C_{(graphite)}$ | Ag | $RbAg_4I_5$ | Te, $AuTe_2$, $AgAu_4Te_{10}$ ($AgAu_3Te_8$) | $C_{(graphite)}$ | Pt (+)
that corresponds the next virtual chemical reaction:
$Ag + 2Te + 4AuTe_2 = AgAu_4Te_{10}$
or
$Ag + 2Te + 3AuTe_2 = AgAu_3Te_8$.

The temperature range of measurements is 332 K – 485 K and the atmospheric pressure of pure argon. The standard thermodynamic properties of krennerite at standard pressure 1 bar ($10^5$ Pa) have the next values: $\Delta_rG^0$ = -96.11 kJ·mol$^{-1}$; $S^0$ = 724.4 J·mol$^{-1}$·K$^{-1}$; $\Delta_rH^0$ = -97.08 kJ·mol$^{-1}$ for $AgAu_4Te_{10}$ composition and $\Delta_rG^0$ = -78.91 kJ·mol$^{-1}$; $S^0$ = 582.7 J·mol$^{-1}$·K$^{-1}$; $\Delta_rH^0$ = -78.46 kJ·mol$^{-1}$ for $AgAu_3Te_8$ composition.

*Keywords: $AuTe_2$, calaverite, $AgAu_4Te_{10}$ ($AgAu_3Te_8$), krennerite, electromotive force method, Ag-Au-Te system.*

## Introduction

In crystallographic studies, krennerite has a chemical formula $Au_{0.8}Ag_{0.2}Te_2$ and belongs to orthorhombic system with space group Pma2 and lattice parameters a=1.658 nm; b=0.8849 nm; c=0.4464 nm (Pertlik, 1984), which corresponds to the composition $AgAu_4Te_{10}$. In mineralogical studies, natural krennerite has a variable composition with the same structural data and the mineral formula $AgAu_3Te_8$ (Dye and Smyth, 2012). But this composition is in disagreement with the phase relationships in the calaverite ($AuTe_2$)-krennerite-sylvanite ($AgAuTe_4$) section of the Ag phase diagram Au-Te (Cabri, 1965), based on the composition of krennerite of $AgAu_4Te_{10}$. At the same time, the krennerite has a region of homogeneity that varies with temperature (Cabri, 1965), but the composition of $AgAu_3Te_8$ is realized only at the peritectic temperature of sylvanite. These contradictions were the reason that the obtained experimental results were recalculated for two compositions in this work.

Theoretical background

For the Gibbs energy of any compound formation it is necessary to get a EMF-temperature dependence of electrochemical reaction. For the different mineral formulas the electrochemical process can be written as follows:

$Ag = Ag^+ + e^-$ left electrode (reference system),
$Ag^+ + e^- + 2Te + 4AuTe_2 = AgAu_4Te_{10}$
or
$Ag^+ + e^- + 2Te + 3AuTe_2 = AgAu_3Te_8$
right electrode (sample system)

---

$Ag + 2Te + 4AuTe_2 = AgAu_4Te_{10}$
total potential-forming reaction (R1a)
or
Ag + 2Te + 3AuTe2 = AgAu3Te8
total potential-forming reaction (R1b).

The reaction (R1) was carried out in an electrochemical cell:

(–)Pt | C(graphite) | Ag | $RbAg_4I_5$ | Te, $AuTe_2$, $AgAu_4Te_{10}$ ($AgAu_3Te_8$) | C(graphite) | Pt(+)(A)

## Experiment

*Reagents.* The next reagents were used for synthesis: powder from Te of zone melting (99.9999%), gold (99.99%), and 0.2 mm thick silver sheet (99.99%). The polycrystalline superionic $RbAg_4I_5$ (99.99%) was fabricated at the Institute for Microelectronics Technology and High-Purity Materials of the Russian Academy of Sciences (Chernogolovka).

*Phase synthesis.* Calaverite and krennerite were obtained by direct synthesis from the elements ("dry synthesis"). The reagents mixture was placed into a quartz glass ampoule that was pumped out to 0.15 Pa and evacuated in the flame of an oxygen burner. Then the substance was heated to melting in the flame of an oxygen burner. The resulting alloy was annealed in a horizontal resistance furnace at a temperature of 623 K during 5 days and cooled at air temperature.

The phase composition of the sample system before and after the experiment was confirmed by X-ray phase analysis: map #85-1310 for $AuTe_2$ (Schutte and De Boer, 1988) and map #75-1413 for $AgAu_4Te_{10}$ ($AgAu_3Te_8$) (Pertlik, 1984).

*Electrode preparation.* Inert electrodes were made from a graphite rod for spectral analysis with a diameter of 6 mm and were connected with a platinum wire. For the reference system electrode a silver pellet ~6 mm in diameter and 3 mm high was used.

A polycrystalline $RbAg_4I_5$ was used as a solid electrolyte. Approximately 0.4 grams of electrolyte powder were pressed at a load of 2.5 tons into a tablet 6 mm in diameter and 3 mm high.

For an electrode of the sample system, the $AuTe_2$ + $AgAu_4Te_{10}$ ($AgAu_3Te_8$) + Te mixture was ground (homogenized) together in an agate mortar and pressed under a load of 2.5 tons into a tablet with a diameter of ~6 mm and a height of 3–4 mm.

*Galvanic cell device.* The cell was assembled in a cell holder in the form of a quartz glass tube (internal

diameter ~6.1 mm). A detailed description of the experimental setup with solid electrolytes and the procedure for working are given in (Voronin, Osadchii, 2011). The measurements were carried out in a flow of dry argon (2-3 $cm^3 \cdot min^{-1}$) to prevent oxidation of cell parts.

**Results**

The experimental values of E(T) of cell (A) are shown in Figure 1.

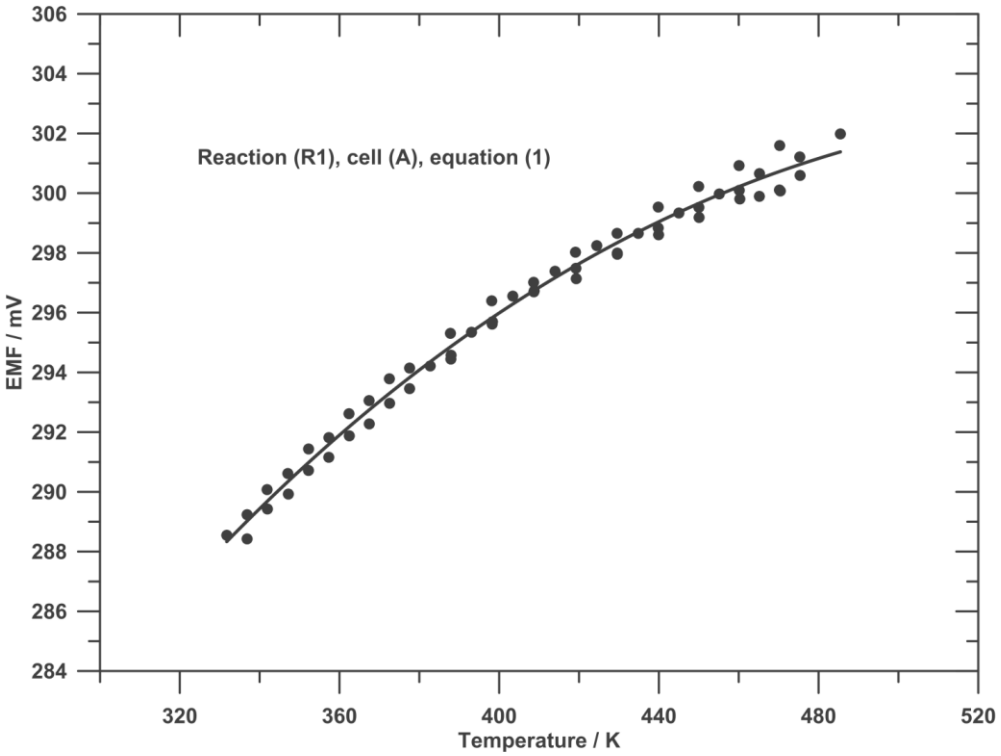


**Fig.1.** EMF - temperature dependence for the cell (A).

E(T) dependence has the form of a smooth logarithmic curve:

$$E(\text{A}), \text{mV} = 157.48 + 1.8886 \cdot T - 0.25743 \cdot T \ln(T), \quad (1)$$
$$(332 < T/\text{K} < 485),\ k = 59,\ R^2 = 0.9896.$$

**Table 2.** Standard thermodynamic values of krennerite (different compositions) and auxiliary data for elements and $AuTe_2$ at 298.15 K and 1 bar pressure.

| Substance | $\Delta_f G°$ ($kJ \cdot mol^{-1}$) | $S°$ ($J \cdot mol^{-1} \cdot K^{-1}$) | $\Delta_f H°$ ($kJ \cdot mol^{-1}$) | Reference |
|---|---|---|---|---|
| Ag | 0 | 42.677 | 0 | Barin, 1995 |
| Au | 0 | 47.497 | 0 | –//– |
| Te | 0 | 49.497 | 0 | –//– |
| $AuTe_2$ | -17.194 | 141.712 | -18.619 | –//– |
| $AgAu_4Te_{10}$ | -96.11 | 724.4 | -97.08 | reaction (R1a) |
| $AgAu_3Te_8$ | -78.91 | 582.7 | -78.46 | reaction (R1b) |

Under the equation there are the measurement temperature range, the number of experimental E/T points (k) and the coefficient of determination (R2). Equation (1) was obtained from the results of 59 E/T points processing by the least squares method.

The next thermodynamic functions can be determined from the temperature dependence of the EMF of the cell (A) using the basic equations of thermodynamics:

$$\Delta_r G\ (J \cdot mol^{-1}) = -nFE \times 10^{-3}$$
$$\Delta_r S\ (J \cdot K^{-1} \cdot mol^{-1}) = nF \cdot (dE/dT) \times 10^{-3}$$
$$\Delta_r H\ (J \cdot mol^{-1}) = -nF \cdot [E - (dE/dT) \cdot T] \times 10^{-3}$$

where n = 1 is the number of electrons involved in the reaction (R1), F= 96485.33289 $C \cdot mol^{-1}$ is the Faraday constant, and E is the EMF value in millivolts.

Using auxiliary data for elements and calaverite taken from (Barin, 1995) (Table 2), the standard thermodynamic properties of krennerite formation from elements at 1 bar ($10^5$ Pa) pressure were calculated:

for $AgAu_4Te_{10}$: $\Delta_f G^0$ = -96.11 $kJ \cdot mol^{-1}$; $S^0$ = 724.4 $J \cdot mol^{-1} \cdot K^{-1}$; $\Delta_f H^0$ = -97.08 $kJ \cdot mol^{-1}$ and for $AgAu_3Te_8$ $\Delta_f G^0$ = -78.91 $kJ \cdot mol^{-1}$; S = 582.7 $J \cdot mol^{-1} \cdot K^{-1}$; $\Delta_f H^0$ = -78.46 $kJ \cdot mol^{-1}$.

Funding source: RFBR 19-05-00482a.

*Acknowledgments:* the authors thank N.A. Drozhzhina for XRD measurements.

**References**

Voronin M.V., Osadchii E.G. Determination of thermodynamic properties of silver selenide by the galvanic cell method with solid and liquid electrolytes // Russian Journal of Electrochemistry, 2011, Vol. 47, No 4, P. 420-426.

Barin I., Thermochemical data of pure substances, Vol. 1 and 2, VCH-Verlag-Ges., 1995

Cabri L.J. Phase relations in the Au-Ag-Te systems and their mineralogical significance // Economic Geology, 1965, Vol. 60, No. 8, P. 1569-1606.

Dye M.D., Smyth J.R. The crystal structure and genesis of krennerite, $Au_3AgTe_8$ // The Canadian Mineralogist, 2012, Vol. 50, No. 1, P. 119-127.

Pertlik F. Crystal chemistry of natural tellurides II: Redetermination of the crystal structure of krennerite, $(Au_{1-x}Ag_x)Te_2$ with x~0.2 // Tschermaks Mineralogische und Petrographische Mitteilungen, 1984, Vol. 33, No 4, P. 253-262.

Schutte W.J., De Boer J.L. Valence fluctuations in the incommensurately modulated structure of calaverite $AuTe_2$ // Acta Crystallographica Section B: Structural Science, 1988, Vol. 44, No. 5, P. 486-494.